ACCSCIENCE PUBLISHING

Tumor Discovery

ORIGINAL RESEARCH ARTICLE

Magnesium-28: A theorical novel self-theranostic strategy targeting metabolic enzyme disruption and intracellular irradiation

Tran Van Luyen*

KLT Research and Application Center, Saigon Scientific and Technological Development Institute, Ong Lanh bridge Ward, Ho Chi Minh City, Vietnam

Abstract

The limitations of conventional cancer therapies, such as low selectivity and significant side effects, necessitate innovative approaches. This study proposes a pioneering self-theranostic strategy using magnesium-28 (Mg-28) alone, enabling simultaneous diagnosis, therapy, and treatment monitoring. Exploiting the elevated Mg ion demand in cancer cells, Mg-28 selectively targets Mg-dependent enzymes (e.g., DNA/RNA polymerases, hexokinase, telomerase) within intracellular organelles, such as the nucleus and mitochondria, without requiring biochemical carriers or nanoparticles, as in recent methods. A theoretical model based on the Mg-uptake coefficient predicts selective Mg-28 accumulation in tumors following intravenous administration. The Mg-28 decay chain—progressing through Aluminum-28 to stable Silicon-28—delivers highly localized irradiation through beta particles, Auger electrons, and recoil ions to critical intracellular structures, while simultaneously disrupting essential Mg-dependent enzymes. This results in a dual mechanism of radiotherapy and multi-enzyme inactivation. Simulations of linear energy transfer, radiation range, and absorbed dose show that nanogram-scale amounts of Mg-28 can deliver 60–400 Gy to tumors ranging from 0.03 mg to 500 g, suggesting potent cytotoxicity across a broad range of tumor sizes and stages. This potential is grounded in the universal metabolic reliance of cancer cells on Mg. Moreover, gamma emissions from Mg-28 and its daughter isotopes support early tumor detection and real-time treatment monitoring, enhancing therapeutic precision. As the first proposed single-isotope theranostic approach leveraging Mg dependency, this innovative strategy provides a robust foundation for future pre-clinical and clinical investigations aimed at validating its therapeutic efficacy, pharmacokinetics, and biosafety—thereby inaugurating a novel hypothesis for cancer therapy.

Keywords: Magnesium-28; Intracellular irradiation; Multienzyme inactivation; Precision metabolic targeting; Self-theranostics; Magnesium uptake

***Corresponding author:**
Tran Van Luyen
(luyen.tranvan@gmail.com)

Citation: Luyen TV. Magnesium-28: A theorical novel self-theranostic strategy targeting metabolic enzyme disruption and intracellular irradiation. *Tumor Discov*. 2025;4(3):70-80. doi: 10.36922/TD025070010

Received: February 10, 2025

1st revised: April 15, 2025

2nd revised: May 2, 2025

3rd revised: May 19, 2025

Accepted: May 21, 2025

Published online: August 13, 2025

Copyright: © 2025 Author(s). This is an Open-Access article distributed under the terms of the Creative Commons Attribution License, permitting distribution, and reproduction in any medium, provided the original work is properly cited.

Publisher's Note: AccScience Publishing remains neutral with regard to jurisdictional claims in published maps and institutional affiliations.

1. Introduction

Cancer remains a paramount global health challenge, responsible for approximately 10 million deaths worldwide in 2020.[1] Despite significant progress in medical oncology, conventional treatment modalities—such as surgery, chemotherapy, radiotherapy, and immunotherapy—are often limited by reduced efficacy in advanced stages, debilitating

systemic side effects, and the persistent issue of tumor relapses due to incomplete eradication of cancer cells.[2]

The advent of targeted therapies, including nanoparticle delivery systems,[3] monoclonal antibodies,[4] peptides,[5] clustered regularly interspaced short palindromic-Cas9,[6] and chimeric antigen receptor-T cells,[7] has improved the precision of cancer cell targeting. However, these approaches predominantly focus on extracellular targets and often require complex delivery mechanisms. A critical gap persists in our ability to effectively target key intracellular processes, particularly the enzymes essential for cancer cell metabolism and replication.

While radioisotopes, such as iodine-131, phosphorus-32, lutetium-177, holmium-166, and yttrium-90 have advanced the field of extracorporeal radiotherapy, including techniques, such as brachytherapy,[2,8] these methods typically rely on carriers to deliver isotopes to the vicinity of tumors and primarily exert their effects extracellularly. As a result, their impact on the intracellular machinery of cancer cells remains limited.[9] For instance, although iodine-131 is effective in treating thyroid cancer, its use carries the risk of inducing secondary malignancies.[10]

A fundamental challenge in current cancer treatment is the failure to comprehensively disrupt the core processes that drive cancer progression, namely, uncontrolled proliferation, limitless replicative potential (immortality), invasion, metastasis, and the sustained energy supply required to support these processes. Intriguingly, all these critical functions are heavily reliant on magnesium ions (Mg^{2+}), which serve as an essential cofactor for numerous Mg-dependent enzymes.[11] Tumor cells characterized by rapid proliferation and heightened metabolic demands, exhibit a significantly elevated requirement for Mg^{2+} compared to normal cells. This metabolic vulnerability presents a unique and underexplored therapeutic opportunity.

Historically, magnesium-28 (Mg-28) has been utilized as a valuable tracer in metabolic studies, particularly in plant biology and in investigations into the pathophysiology of diabetes.[12-14] However, it's potential as a therapeutic agent for cancer remains largely unexplored. This study introduces Mg-28 as a dual-action agent that combines targeted intracellular irradiation with the direct inactivation of Mg-dependent enzymes. A potential concern regarding the use of Mg-28 stems from the fact that Mg^{2+} is a cofactor for over 300 enzymes, raising questions about potential off-target effects in vital organs, such as the lungs, liver, and brain. However, this research demonstrates the contrary: Mg-28 exhibits a strong propensity to selectively concentrate on malignant tumors—the very sites where cell survival, proliferation, invasion, and metastasis require Mg levels far exceeding those of healthy tissues. Following intravenous administration, Mg-28 is hypothesized to selectively accumulate within these tumor cells, competitively replacing stable Mg^{2+} in crucial enzymes. The subsequent decay of Mg-28 emits beta particles, Auger electrons, and recoil ions that directly target intracellular structures, such as the nucleus and mitochondria. This dual mechanism aims to overcome therapeutic resistance, minimize off-target effects, and enable self-theranostic applications by integrating both therapy and diagnostics within a single agent.

The overarching objective of this work is to comprehensively analyze the Mg-28 approach and demonstrate its feasibility as a groundbreaking strategy that combines the precision of targeted intracellular chemotherapy with radiotherapy, while minimizing damage to healthy tissues and enabling early diagnosis and dynamic monitoring of therapeutic progress. This research seeks to unlock the transformative potential of Mg-28 as a next-generation theranostic platform in the ongoing fight against cancer. In fact, this approach may serve as a foundation for pre-clinical and clinical evaluation in the future.

2. Methodology

This theoretical study evaluates the feasibility of Mg-28 as a precision cancer therapy through a comprehensive analysis encompassing five key aspects: (1) The fundamental principles of metalloenzyme inactivation; (2) the mechanism of Mg-dependent multienzyme disruption due to changes in cofactor valence and ionic radius; (3) the calculation of linear energy transfer (LET) and the range of emitted radiation particles, including recoil effects; (4) the quantification of absorbed dose in tumors of varying volumes and the assessment of systemic dose; and (5) the tumor-specific uptake of Mg ions driven by the metabolic demands of cancer cells. This approach builds upon the basic principles of metalloenzyme inactivation detailed in our previous publications.[15,16]

2.1. Principles of metalloenzyme inactivation

The strategy is based on the substitution of stable metal ion cofactors in metalloenzymes with suitable radioisotopes to induce enzyme inactivation. Ideal radioisotopes for this purpose should emit beta particles or Auger electrons and possess a half-life ($T_1/_2$) that is neither excessively long (to minimize prolonged radiation exposure) nor too short (to allow for clinical utility). Furthermore, their decay products should be isotopes of elements that do not function as cofactors at the enzyme's active site. Mg-28 ($T_1/_2 \approx 21$ h) meets these criteria for targeting Mg-dependent enzymes, decaying into Aluminum-28 (Al-28) and subsequently

Silicon-28 (Si-28), with emissions capable of disrupting the function of these critical enzymes in cancer cells.[17]

2.2. Mechanism of Mg-dependent enzyme inactivation

Mg^{2+} typically stabilizes the active sites of Mg-dependent enzymes by forming six-coordinate bonds with oxygen atoms from carboxylate and phosphate groups.[18-21] This coordination is essential for substrate binding and catalytic activity. Upon radioactive decay, Mg-28 transforms into Al^{3+} and then Si^{4+}, both of which possess higher charges and smaller ionic radii (Al^{3+}: 0.50 Å; Si^{4+}: 0.40 Å) compared to Mg^{2+} (0.72 Å).[22,23] This substitution disrupts the electrostatic interactions within the active site, leading to structural stress, distortion, weakened substrate binding, and ultimately, impaired or abolished catalytic efficiency. In addition, the recoil of Al-28 and Si-28 ions during decay (with a displacement of 0.022–1.5 Å) can cause local distortions at the enzyme active site. Given the precise spatial requirements for enzymatic catalysis, such displacements can further impair enzyme functionality. The high-LET particles (beta particles and Auger electrons) emitted during decay also contribute to enzyme inactivation by breaking covalent and non-covalent bonds within the apoenzyme and generating free radicals that denature surrounding proteins.

2.3. LET and radiation range

The LET and the range of beta particles, Auger electrons, and recoil ions emitted during Mg-28 decay were calculated using the NIST ESTAR program[24] and Medical Internal Radiation Dose (MIRD) data.[17,25] For recoil ions (Al-28 and Si-28), recoil energies were derived using Equation I, based on the principle of conservation of momentum following beta particle emission from the parent Mg-28 nucleus.

$$E_{recoil} = \frac{E_{\beta}^2}{2Mc^2} \quad \text{(I)}$$

where E_{recoil} is the recoil energy of the daughter nucleus (Al-28 or Si-28); E^{β} is the energy of the emitted beta particle; M is the mass of the daughter nucleus; and $c^2 = 9 \times 10^{16}\ m^2/s^2$ is the square of the speed of light.

These resulting energy values were then used to model the LET and range of these recoil ions in different tissue types.

2.4. Absorbed dose calculations

Absorbed dose calculations were performed for tumors of different volumes (T_0–T_5) and for the whole body of a 60-kg individual using the MIRD program[26] and publicly available nuclear data.[17,25] Modeled scenarios assumed the administration of Mg-28 in doses ranging from 0.1 to 6.2 ng and included three delivery scenarios: (1) Intravenous injection without tumor-specific uptake, (2) intravenous injection with high tumor-specific uptake (based on the Mg uptake coefficient of tumor cells), and (2) direct injection into the tumor. In addition, absorbed doses were evaluated for different treatment regimens involving 62, 300, and 400 Mg-28 ions/cell. These correspond to different levels of inhibition, with the aim of inactivating approximately 300 Mg-dependent enzymes.

2.5. Tumor-specific Mg uptake

The selective accumulation of Mg^{2+} by cancer cells, compared to their normal counterparts, forms the foundation for employing the radioisotope Mg-28 in targeted cancer therapy. This differential uptake arises primarily from the significantly higher replication rates of cancerous tissues, leading to an increased demand for Mg^{2+}—a crucial cofactor for numerous enzymes involved in DNA replication, protein synthesis, and energy metabolism.[11,20] Although intracellular concentrations of stable Mg^{2+} may be similar in individual normal and cancerous cells, the dynamic process of rapid cell division leads to a significantly greater overall Mg^{2+} uptake at the tissue level in tumors.

To quantify this difference, we model the reproductive capacity of healthy and cancerous tissues over time. The proliferation of healthy and cancerous tissues can be calculated using Equations II and III, respectively, while the growth ratio between the two types of tissues is expressed as in Equation IV.

$$Healthytissue: A = 2^{(n_a)}; \left(n_a = t/T_a \right) \quad \text{(II)}$$

$$Cancer\ tissue: B = 2^{(n_b)}; \left(n_b = t/T_b \right) \quad \text{(III)}$$

$$B/A = 2^{(n_b - n_a)} = 2^{t(1/Tb - 1/Ta)} \quad \text{(IV)}$$

where A and B are the number of healthy cells and cancer cells, respectively; n_a and n_b are the number of doubling periods of healthy tissue and cancerous tissue, respectively; t is the actual copy time; and T_a and T_b are the replication cycle of healthy cells and cancer cells, respectively.

By introducing the doubling time ratio $k = T_a/T_b$, which reflects the differences in cell division dynamics, Equation IV can be transformed to Equation V.

$$B/A = 2^{t/T_b \times (1-1/k)} \quad \text{(V)}$$

where A and B are the number of healthy cells and cancer cells, respectively; t is the actual copy time; T_b is the replication cycle of cancer cells; and k is the doubling time ratio.

Unlike normal cells, cancer cells are not regulated by cyclin-dependent kinases,[27] which ensure genomic integrity, accurate protein synthesis, and complete DNA repair in healthy cells. For this reason, their replication is faster—resulting in k >1.

Rapid replication in cancer cells creates a disproportionately high demand for resources essential for survival and division, including Mg^{2+}. This demand doubles during the M phase of the cell cycle. Therefore, this ratio, when normalized to the initial number of cells, is known as the Mg-28 uptake coefficient. This preferential Mg uptake by cancer cells is the cornerstone of the Mg-28 therapy. The elevated demand for Mg^{2+} in rapidly dividing cancer cells acts as a natural driving force for the selective accumulation of the Mg-28 radioisotope within the tumor microenvironment. This intrinsic targeting mechanism eliminates the need for complex biochemical carriers or nanoparticles, simplifying the treatment process and reducing potential off-target toxicities. The high Mg-uptake coefficient not only enhances the intracellular delivery of Mg-28 for enzyme inactivation and irradiation but also underpins its potential for early diagnosis and real-time monitoring, as even small tumors exhibit a measurable increase in Mg accumulation. This coefficient is also the basis for calculating absorbed doses and enzyme inactivation in intravenous treatment regimens, where energy transfer from Mg-28 decay within the cancer cell microenvironment leads to the disruption of molecular bonds.

3. Results

3.1. Mg-uptake coefficient

The Mg-uptake coefficient (B/A), a key determinant of Mg-28 distribution, was calculated by Equation V with an assumed value of k = 2. The results demonstrate a significant increase in the coefficient with tumor size and the number of replication cycles.

As demonstrated in Table 1, the coefficient increases dramatically with the number of replication cycles (n_b) and the value of k. For instance, even with a modest k value of 2, the Mg-uptake coefficient escalates from 1.8×10^2 at 15 cycles (T_0 tumor) to 7.1×10^5 at 39 cycles (T_5 tumor). This highlights the profound ability of growing tumors to selectively accumulate Mg ions. This trend reflects the elevated Mg demand of rapidly proliferating cancer cells, which enhances the selective targeting of Mg-28 to larger and more metabolically active tumors compared to smaller or less active ones, and significantly more than to normal cells.

3.2. LET and particle range

The LET values and corresponding ranges for the particles emitted during Mg-28 decay are presented in Table 2 and illustrated in Figure 1.

Electron Auger, Beta particles (β), and recoiled ions[26,27]

Electron Auger of Mg-28 is KLL(Mg-28); E = 0.0014 MeV

Electron Auger (1) of Al-28 is (Al-28) KLL; E = 0.00159 MeV

Electron Auger (2) of Al-28 is (Al-28) KLX; E = 0.00170 MeV

Electron Auger (3) of Al-28 is (Al-28) KXY; E = 0.00181 MeV

β1 Mg-28 E = 0.0659 MeV

β 2 Mg-28 E = 0.1559 MeV

β 3 Mg-28 E = 0.3192 MeV

β Al-28 E = 1.124 MeV

Recoiled ion Al-28: from β1 of Mg-28; E = 0.0039 eV

Recoiled ion Al-28: from β2 of Mg -28; E = 0.0109 eV

Recoiled ion Al-28: from β3 of Mg -28; E = 0.0366 eV

Recoiled ion Si-28: from β1 of Al-28; E = 0.*171 eV*

Beta-minus particles exhibit LET values of 0.002–0.09 eV/Å with a range of 0.07–6.11 mm. Auger electrons demonstrate higher LET values, ranging 0.81–1.6 eV/Å, but with a shorter range of 88–224 nm. Recoil ions (Al-28 and Si-28) have LET values between

Table 1. Tissue characteristics and magnesium-28 absorbtion coefficient

Content	Tissue level					
	T_0	T_1	T_2	T_3	T_4	T_5
Mass (g)	3.1E-05	5.0E-03	5.0E-02	5.0E-01	5.0E+00	5.0E+02
Number of cells	3.1E+04	5.0E+06	5.0E+07	5.0E+08	5.0E+09	5.0E+11
Number of cell cycles, n_b	15	22	27	29	32	39
Absorption coefficient	1.8E+02	3.2E+03	7.1E+03	2.2E+04	7.1E+04	7.1E+05

Notes: T_0 was defined using Equation III after n_b=15 cycles, where $B = 2^{n_b}$ and $\left(n_b = t/T_b\right)$. The absorption coefficient is calculated based on the cumulative uptake over successive cell cycles, assuming k=2.

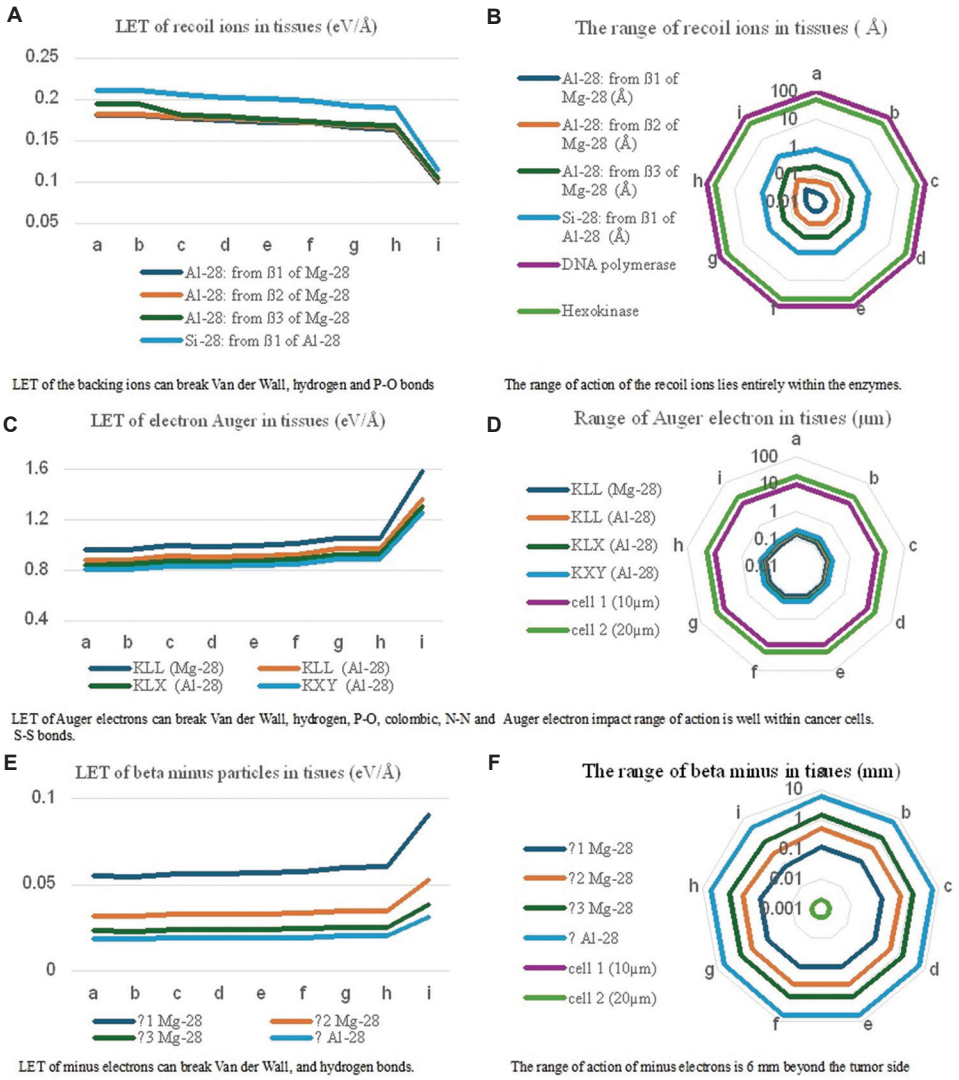


Figure 1. LET and range of different particles in biological tissues, derived from Table 2 and Table 3. (A and B) LET and range of recoil ions from Mg-28 and Al-28 decay. LET of the recoil ions can break Van der Wall, hydrogen, and P-O bonds, and their range of action lies entirely within the enzymes. (C and D) LET and range of Auger electrons from electron shell transitions (KLL, KLX, KXY). LET of Auger electrons can break Van der Wall, hydrogen, P-O, coulombic, N-N, and S-S bonds, and their impact range of action is well within cancer cells. (E and F) LET and range of beta-minus particles from different isotopes of Mg-28 and Al-28. LET of the electrons can break Van der Wall and hydrogen bonds, and their range of action is 6 mm beyond the tumor side. Labels (a-i) indicate different tissue types: (a) Water; (b) Soft tissue (ICRP); (c) brain; (d) Musculoskeletal (ICRP); (e) lung; (f) blood; (g) skin (ICRP); (h) M-E liquid, Sucrose; (i) Cortical bone (ICRP). Abbreviations: Al-28: Aluminium-28; ICRP: International Commission on Radiological Protection; KLL, KLX, KXY: Auger electron transitions between electron shells (K, L, X, Y); LET: Linear energy transfer; M-E: Mass-equivalent; Mg-28: Magnesium-28; P–O: Phosphorus-oxygen; S–S: Sulfur-sulfur.

Table 2. LET and range of Auger electrons, beta-minus particles, and recoil ions

Particle	LET (eV/Å)	Range
Auger electron	0.81–1.6	88–224 nm
Beta minus	0.002–0.09	0.07–6.11 mm
Recoil ion	0.1–0.21	0.022–1.5 Å

Notes: LET is expressed in eV/Å, equivalent to keV/µm using the conversion factor 1 keV/µm=0.1 eV/Å. Conversion constants: 1 keV=10^3 eV; 1 MeV=10^6 eV; 1 µm=10^3 nm=10^4Å.
Abbreviation: LET: Linear energy transfer.

0.1 eV/Å and 0.21 eV/Å and a very short range of 0.022–1.5 Å. The values in Table 3 indicate that Auger electrons possess the highest LET and medium range, enabling them to effectively break a variety of molecular bonds within tumor cells. Examples of such bonds include Van der Waals, hydrophobic, coulombic, P-O (ATP/ADP), N-N, and S-S bonds. Recoil ions, despite their limited range and relatively weaker overall effect, can effectively disrupt enzyme bonds due to their highly localized action at the molecular level, targeting coulombic, hydrophobic, and

Van der Waals bonds. In contrast, beta-minus particles, due to their long range and lowest LET, primarily affect hydrophobic and Van der Waals bonds and produce free radicals along their path. The therapeutic impact can thus be characterized by the focused molecular-level action of recoil ions, the intracellular effect of Auger electrons, and the extended influence of beta-minus particles up to 6mm beyond tumor margins. These distinctions are further illustrated in Figure 1.

3.3. Absorbed dose

Absorbed dose calculations by the MIRD code,[26] with 0.1 ng of Mg-28 administered intravenously over 21 h (Table 4), showed the potential for highly effective tumor cell killing with minimal impact on healthy tissues. Three regimens were modeled: (a) Whole-body cell dose, (b) Mg-uptake coefficient-based cell dose, and (c) direct tumor cell dose. In regimen (a), the doses ranged from

Table 3. Impact of linear energy transfer (LET) from magnesium-28 (Mg-28) decay on the dissociation of biological molecular bonds

Bond type	Length (Å)	Bond energy (kJ/mol)	Beta minus (kJ/mol)	Auger electron (kJ/mol)	Recoiled ions (kJ/mol)
Van der Waals	3.0–4.0	~ 2.4–4	7.08–34.84	311.81–612.41	38.12–81.08
Hydrogen bond	1.5–2.0	~4–40	3.54–17.42	155.91–306.21	19.06–40.54
P–O (in ATP/ADP)[28]*	~1.60	~30.5	2.83–13.94	124.72–244.96	15.25–32.43
Ionic	2.0–4.0	~20–200	7.08–34.84	311.81–612.41	38.12–81.08
N–N	~1.45	~163	2.57–12.63	112.88–222.00	13.82–29.39
S–S	2.05	~250	3.64–17.82	156.31–381.20	19.46–41.54

Notes: (1) *Bond energy released when ATP hydrolyzes to ADP; 1eV=96.485 kJ/mol. (2) Van der Waals interactions (3.0–4.0 Å) are weak but critical for stabilizing protein side chains and stacked DNA bases. Hydrogen bonds (1.5–2.0 Å) maintain DNA base pairing (A=T, G≡C) and play a key role in enzyme-substrate interactions. Ionic (Coulombic) interactions (2.0–4.0 Å) are prominent between oppositely charged side chains of proteins and in ATP–Mg^{2+}coordination complexes. Phosphodiester (P–O) bonds (~1.60 Å) form the DNA/RNA backbone and are targets for strand cleavage during radiation damage. Disulfide bridges (S–S) (~2.05 Å) stabilize the tertiary/quaternary structure of many enzymes, particularly in oxidative environments. Nitrogen–nitrogen (N–N) bonds (~1.45 Å) are present in some nucleotide base pairs and enzyme cofactors (e.g., flavins). The LET values from Mg-28 decay are sufficient to break all the above interactions, directly impairing nucleic acid integrity and enzymatic function essential to cellular integrity, especially in cancer cells.

Table 4. Absorbed dose to tumors across different regimens and the amount of magnesium-28 (Mg-28) required

Content	Regimen	Cancer type					
		T_0	T_1	T_2	T_3	T_4	T_5
Number of cells		3.28E+04	5.00E+06	5.00E+07	5.00E+08	5.00E+09	5.00E+11
Intravenous cell dose, uniformly distributed throughout the body (Gy)	a	1.01E-11	1.55E-09	1.55E-08	1.55E-07	1.55E-06	1.55E-04
Intravenous cell dose with Mg absorption coefficient (Gy)	b	1.83E-09	3.46E-06	1.09E-04	3.46E-03	1.09E-01	1.09E+02
Cell dose injected directly into the tumor (Gy)	c	3.04E+04	2.23E+02	2.23E+01	2.23E+00	2.23E-01	2.23E-02
Tumor dose (Gy)	a	3.31E-07	7.75E-03	7.75E-01	7.75E+01	7.75E+03	7.75E+07
	b	6.00E-05	11.15E+00	11.15E+03	11.15E+05	11.15E+08	11.15E+13
	c	9.97E+08	38.75E+08	38.75E+08	38.75E+08	38.75E+08	38.75E+09
	d	6.01E+01	6.01E+01	6.01E+01	6.01E+01	6.01E+01	6.01E+01
	e	3.12E+02	3.12E+02	3.12E+02	3.12E+02	3.12E+02	3.12E+02
	f	4.15E+02	4.15E+02	4.15E+02	4.15E+02	4.15E+02	4.15E+02
Whole-body absorbed dose (Gy)	d	3.52E-01	2.03E-02	8.91E-03	2.82E-03	8.91E-04	8.91E-05
	e	1.72E+00	9.81E-02	4.42E-02	1.44E-02	4.42E-03	4.42E-04
	f	2.33E+00	1.32E-01	5.92E-02	1.92E-02	5.92E-03	5.92E-04
Amount of Mg-28 required (ng)	d	9.31E-01	5.33E-02	2.42E-02	7.51E-03	2.44E-03	2.44E-04
	e	4.62E+00	2.63E-01	1.22E-01	3.71E-02	1.22E-02	1.22E-03
	f	6.21E+00	3.51E-01	1.63E-01	5.04E-02	1.63E-02	1.63E-03

Note: All absorbed dose calculations are based on a 21-h decay duration. Regimen (d) assumes 62 Mg-28 ions/cell, regimen (e) assumes 300 ions/cell, and regimen (f) assumes 400 ions/cell.

10^{-11} to 10^{-4} Gy for T_0–T_5 tumors (0.03 mg–500 g). For the same tumors, the doses increased from 10^{-9} to 10^{2} Gy in regimen (b) but decreased from 10^{4} to 10^{-2} Gy in regimen (c). These results indicate that applying the Mg-uptake coefficient significantly increases the cell dose compared to a uniform whole-body distribution.

Based on these results, we proposed three additional intravenous regimens: (d) 62, (e) 300, and (f) 400 Mg-28 ions/cell. These regimens were capable of targeting 20%, 100%, and 133% of the total 300 Mg-dependent enzymes, respectively. They achieved absorbed doses ranging from 60 to 415 Gy across T_0–T_5 tumors, with a total Mg-28 quantity of only 6.2 ng. Notably, the highest effective systemic absorbed dose among the regimens remained below 2.4 Gy, indicating a favorable safety profile. These results demonstrate that Mg-28 delivers sufficient absorbed doses to induce significant cytotoxicity in cancer cells across a wide range of tumor sizes, with minimal damage to surrounding healthy tissues and limited overall radioisotope exposure. These results are shown in Figure 2.

4. Discussion

4.1. Tumor growth, replication cycle, and Mg uptake

Cancer cell replication cycles are known to vary depending on tumor type and microenvironmental conditions. Our data, presented in Table 1, indicate a clear relationship between tumor size, the number of replication cycles, and the Mg-uptake coefficient. For instance, a microscopic tumor at stage T_0 (mass ~3.1×10^{-5} g, approximately 3.1×10^{4} cells) after 15 replication cycles exhibits an Mg-uptake coefficient of 1.8×10^{2}. As the tumor progresses through stages T_1–T_5, with increasing mass and number of replication cycles, the Mg-uptake coefficient demonstrates a significant upward trend, reaching 7.1×10^{5} for a large T_5 tumor (mass ~500 g, ~5.0×10^{11} cells) after 39 cycles, assuming a replication cycle ratio (k) of 2 between cancerous and healthy tissue.

This substantial increase in the Mg-uptake coefficient with tumor growth underscores the elevated Mg demand of rapidly proliferating cancer cells. As tumors expand, their metabolic and replicative requirements for Mg—a crucial cofactor for numerous enzymes involved in these processes—escalate. Consequently, Mg-28 is preferentially accumulated in larger and more aggressive tumors, making it an increasingly effective agent for targeted radiotherapy in advanced stages.

Furthermore, the relatively high Mg-uptake coefficient observed even in early-stage T_0 tumors suggests a promising avenue for early cancer detection, which will be discussed further in the subsequent section. The dependence of the Mg-uptake coefficient on the number of replication cycles and the k-factor highlights the importance of considering tumor growth dynamics in optimizing Mg-28-based treatment strategies. Tumors with faster replication rates (higher k values) are expected to exhibit even greater Mg-28 accumulation, potentially enhancing therapeutic efficacy and reducing the required dosage.

4.2. Early diagnosis and real-time monitoring

The exceptionally high Mg-uptake coefficient observed even in early-stage, microscopic tumors (T_0: 1.8×10^{2}, as shown in Table 1) provides a strong foundation for early cancer diagnosis. This preferential accumulation of Mg-28 in nascent tumors allows for robust imaging signals through gamma rays, Bremsstrahlung, and X-rays, enabling detection through positron emission tomography (PET) or single-photon emission computed tomography (SPECT) imaging. The ability to visualize tumors as small as ~3.1×10^{-5} g (approximately 31,000 cells) represents a significant advancement over many current diagnostic

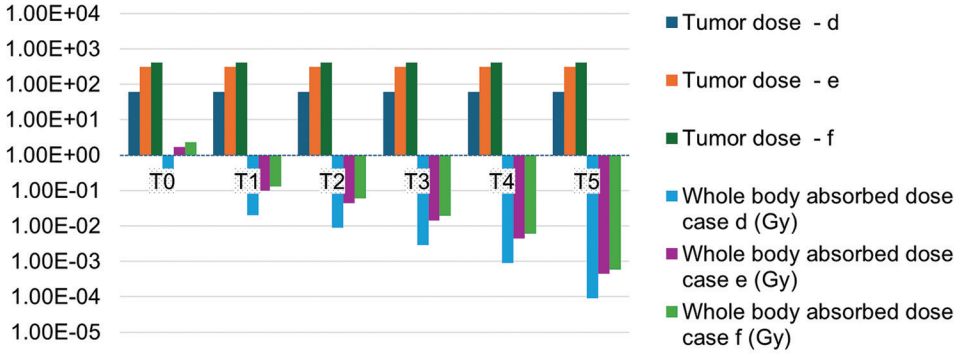


Figure 2. Comparison of absorbed radiation dose delivered to tumors and the whole body across different regimens. The tumor-specific and systemic absorbed dose are computed from Table 4. Regimens d, e, and f correspond to assumptions where 62, 300, and 400 magnesium-28 ions were taken up per cancer cell to inactivate magnesium-dependent enzymes. Tumor doses range between 60 Gy and 415 Gy, while whole-body doses are from 1.0×10^{-4} Gy to 2.4 Gy, indicating high therapeutic selectivity and patient safety.

modalities that may only detect larger tumor masses. Traditional methods usually diagnose cancer at the milligram scale using PET-computed tomography (CT) or SPECT-CT.[2,8,9]

Moreover, the continuous uptake of Mg-28 by tumor cells, sustained throughout the treatment period, facilitates real-time monitoring of therapeutic response. Changes in Mg-28 concentration within the tumor, as visualized through imaging, can provide immediate feedback on treatment efficacy, allowing for timely adjustments to the therapeutic regimen. This dual diagnostic and therapeutic (theranostic) functionality, achieved with a single isotope, simplifies the clinical workflow and eliminates the need for paired diagnostic and therapeutic agents, representing a key advantage of the Mg-28 method. Current methods often use two or more radioactive isotopes for diagnosis and treatment monitoring, such as Tc-99m + Y-90 or Tc-99m + Lu-177 with SPECT-CT, and F-18 + Y-90 or F-18 + Lu-177 with PET-CT.[2,8,9]

4.3. Enzyme inactivation and intracellular irradiation

Data from Table 2 reveal the LET and range of the particles emitted during Mg-28 decay. Auger electrons exhibit the highest LET (0.81–1.6 eV/Å), followed by recoil ions (0.1–0.21 eV/Å), while beta-minus particles have a lower LET (0.002–0.09 eV/Å) but a much longer range (0.07–6.11 mm).

The high LET of Auger electrons and recoil ions is particularly significant for enzyme inactivation and intracellular damage. As shown in Table 3, the energy deposited by these particles per unit length is sufficient to break various critical biological bonds, including the relatively strong covalent bonds, such as S-S (disulfide) and P-O (in ATP/ADP), as well as weaker non-covalent bonds, such as Van der Waals and hydrogen bonds that are crucial for maintaining the three-dimensional structure and function of enzymes and DNA. The recoil of Al-28 and Si-28 ions, although occurring over a very short range (0.022–1.5 Å), can directly disrupt the active sites of enzymes due to the momentum transfer and local structural distortion. These effects, together with the difference in charge and ionic radius from Mg^{2+} to Al^{3+} to Si^{4+}, will certainly inactivate Mg-dependent enzymes once Mg-28 replaces stable Mg in these enzymes. Specifically, the inactivation of DNA/RNA polymerases, helicase, topoisomerase, and DNA repair enzymes disrupts or arrests the S phase of the cell cycle, leading to apoptosis. Targeting telomerase prevents cancer cells from achieving immortality, thus limiting tumor growth and reducing the potential for invasion. Furthermore, the inactivation of matrix metalloproteinases (MMPs) impairs the ability of cancer cells to invade surrounding tissues and metastasize. By disrupting key metabolic enzymes, such as hexokinase, kinases, and ATPases, Mg-28 deprives cancer cells of essential energy, leading to metabolic collapse and necrosis.

Beta-minus particles, despite their lower LET, have a longer range that allows them to traverse larger cellular distances, generating free radicals along their path. These free radicals can indirectly damage DNA, proteins, and other cellular components, contributing to the overall cytotoxic effect of Mg-28. The combined action of direct bond breakage by high-LET particles and indirect damage by free radicals ensures a multifaceted attack on essential cellular machinery.

Targeted irradiation within the nucleus and mitochondria is achieved through the selective uptake of Mg-28, where crucial Mg-dependent enzymes, such as DNA/RNA polymerases, hexokinase, and telomerase reside. The subsequent decay of Mg-28 directly induces localized irradiation through beta particles, Auger electrons, and recoil ions, resulting in a concentrated release of damaging particles close to their molecular targets, thus maximizing enzyme inactivation and cellular destruction. Traditional inhibitors or modern methods[3-7] usually use one inhibitor for one specific enzyme or one biochemical agent for one determined molecular target.

4.4. Precision targeting and safety profile

The distinct ranges of the emitted particles from Mg-28 decay contribute to its precision targeting and favorable safety profile. The very short range of recoil ions (0.022–1.5 Å) ensures that their destructive energy is deposited within nanometer distances, primarily affecting the enzyme molecules in their immediate vicinity. Auger electrons, with a slightly longer range (88–224 nm), also deposit their energy within the subcellular compartments, causing localized damage to organelles, such as the nucleus and mitochondria.

In contrast, the longer range of beta-minus particles (up to 6.11 mm) might suggest the potential for off-target effects. However, the preferential uptake of Mg-28 by cancer cells, as indicated by the high Mg-uptake coefficient, concentrates the source of these beta particles within the tumor tissue. Furthermore, the energy deposition per unit length (LET) of beta-minus particles is lower compared to Auger electrons and recoil ions, meaning that while they can travel further, the density of ionization events along their path is less intense. This localized delivery of radiation, particularly the high-LET emissions within the tumor cells, minimizes the exposure of surrounding healthy tissues to significant radiation doses.

The absence of a need for bulky biochemical carriers or nanoparticles further enhances the precision and safety of Mg-28 therapy. As a naturally recognized ion, Mg-28 is efficiently transported into cancer cells, ensuring direct intracellular irradiation without the complexities and potential drawbacks of exogenous delivery systems. This intrinsic targeting mechanism contributes to the high local dose within the tumor while minimizing systemic toxicity.

4.5. High local dose with minimal systemic toxicity

Simulation results using the MIRD code (Table 4) demonstrate the potential of Mg-28 to deliver a high absorbed dose to tumors while maintaining minimal systemic toxicity. The calculations, performed over 21 h (approximately one half-life of Mg-28), considered different treatment regimens based on the number of Mg-28 ions internalized per cancer cell.

Assuming a regimen of 400 Mg-28 ions/cell (regimen f), a tumor absorbed dose of 415 Gy can be achieved across all tumor stages (T_0–T_5). This dose is significantly above the generally accepted therapeutic threshold of around 50 Gy required for effective tumor control. Notably, the total amount of Mg-28 needed to deliver this high local dose is remarkably small, with a maximum of only 6.2 ng required for even the largest T_5 tumors. This high efficacy at the nanogram scale underscores the potency and economic viability of the Mg-28 approach.

Conversely, the corresponding whole-body absorbed dose for the same regimen (regimen f) remains consistently low, with a maximum of 2.33 Gy observed for the smallest T_0 tumors, decreasing to the mGy range for larger tumors (e.g., 59.2 mGy for T_2 and 5.92 mGy for T_4). This significant disparity between the high local tumor dose and the low systemic exposure highlights the inherent safety advantage of Mg-28 therapy, minimizing potential damage to healthy organs and tissues.

The enhanced Mg uptake by cancer cells, driven by their elevated metabolic and replicative demands, further contributes to this favorable dose distribution. This biological preference ensures that Mg-28 is selectively concentrated within the tumor microenvironment, maximizing the therapeutic effect while sparing normal cells.

The data in Table 4 also illustrate the dose-response relationship with varying numbers of Mg-28 ions/cell (regimens d, e, and f). Even with lower intracellular concentrations of Mg-28 (62 and 300 ions/cell), therapeutically relevant tumor doses (60.1 Gy and 312 Gy, respectively) can be achieved with correspondingly lower systemic exposure and amounts of Mg-28 required. This flexibility in dosing regimens allows for tailored treatment strategies based on tumor characteristics and patient-specific factors.

4.6. Summary of key advantages

The Mg-28 therapy presents a transformative and biologically intelligent approach to cancer treatment, offering several key advantages that distinguish it from conventional modalities.

4.6.1. Dual mechanism of action for enhanced efficacy

By simultaneously targeting multiple critical Mg-dependent enzymes essential for cancer cell survival and proliferation (DNA/RNA polymerases, hexokinase, telomerase, and MMPs) and delivering highly localized intracellular irradiation through its decay products (beta particles, Auger electrons, and recoil ions), Mg-28 offers a synergistic therapeutic effect. This can overcome drug resistance and achieve comprehensive tumor control—a key advantage over single-target traditional inhibitors.

4.6.2. Intrinsic and highly selective tumor targeting

The therapy leverages the inherent metabolic vulnerability of cancer cells, characterized by their rapid proliferation and elevated demand for Mg. The quantified Mg-uptake coefficient demonstrates a significant preferential accumulation of Mg-28 within tumor tissues, eliminating the need for complex and potentially toxic biochemical carriers or nanoparticles. This natural targeting mechanism ensures a high concentration of the therapeutic agent directly within the tumor microenvironment.

4.6.3. Integrated self-theranostic capability

Mg-28 uniquely combines diagnostic and therapeutic functionalities within a single radioisotope, embodying a self-theranostic approach. Its gamma emissions allow for early tumor detection using PET or SPECT imaging—even at microscopic stages—while its continuous uptake facilitates real-time monitoring of treatment response, enabling personalized and adaptive therapeutic strategies without the need for additional agents.

4.6.4. Maximized local efficacy with minimized systemic toxicity

Simulation data indicate that Mg-28 can deliver cytotoxic radiation doses directly to tumor cells at the nanogram scale, while the absorbed dose to surrounding healthy tissues remains remarkably low. This favorable therapeutic index is attributed to the selective tumor uptake and the short-range, high-LET emissions of its decay products, which concentrate the destructive energy within the tumor volume.

4.6.5. Broad applicability and potential for expanded therapeutic horizons

The fundamental principle of exploiting the increased metabolic demands of rapidly dividing cells suggests that Mg-28 therapy holds promise across a wide spectrum of cancer types and stages. In addition, the concept of targeting host cell enzymes essential for pathogen replication opens avenues for exploring its utility in treating other diseases, such as viral infections—including coronaviruses that rely on host cell RNA polymerase for replication. Furthermore, this approach may be extended to other cofactors, such as copper, iron, manganese, zinc, and selenium.

5. Conclusion and future directions

The Mg-28 method represents a revolutionary and multifaceted approach to cancer therapy, characterized by its dual mechanism of action: The targeted inactivation of crucial Mg-dependent enzymes and highly localized intracellular irradiation.

The intrinsic selectivity of this approach is biologically elegant, driven by the elevated Mg demand of rapidly proliferating cancer cells. This phenomenon, quantified by the Mg-uptake coefficient, allows for natural tumor targeting without the need for complex biochemical carriers or nanoparticles—thereby enhancing both treatment precision and safety.

Preliminary analytical modeling and LET-dose simulations support the foundational hypothesis, demonstrating that nanogram-scale doses of Mg-28 can achieve therapeutic cytotoxic thresholds. Importantly, the behavior of Mg-28 within the tumor microenvironment embodies a form of natural biological targeting, where cancer cells, fueled by their metabolic and replicative demands, act as selective attractors for Mg^{2+}. This pathway allows Mg-28 to efficiently infiltrate intracellular compartments, particularly the nucleus and mitochondria, where it disrupts the enzymatic machinery critical for cancer progression.

Furthermore, the inherent gamma emissions of Mg-28 confer an integrated self-theranostic capability, enabling early tumor detection and real-time monitoring of treatment response, thus offering unparalleled precision in cancer management. Significantly, this approach holds promise for application across all cancer types and stages, a distinct advantage over many existing therapies. Beyond oncology, the principle of targeting host cell enzymes extends to infectious diseases. For instance, Mg-28 may disrupt the replication cycle of viruses—such as coronaviruses—by inactivating host RNA polymerase, thus offering a novel antiviral strategy. This innovative approach sets a strong foundation for future research and deserves in-depth exploration through pre-clinical (*in vitro* and *in vivo*) and clinical studies to evaluate its efficacy, pharmacokinetics, and biosafety. Ultimately, Mg-28 therapy could inform the development of a new paradigm in cancer and infectious disease treatment.

Despite its promising potential, several challenges must be addressed to translate Mg-28 therapy from theory to practice. The clinical safety and therapeutic efficacy require extensive, rigorous validation. In addition, Mg-28 production is costly and technically complex, and the clinical trials and regulatory approval processes demand significant logistical and financial investments. The short half-life of Mg-28 necessitates extremely rapid and efficient transportation and administration systems to ensure effective delivery.

To overcome these challenges and pave the way for clinical translation, the following strategic actions are recommended on duct: (1) Conduct *in vitro* and *in vivo* studies to validate the model; (2) establish cancer treatment centers near nuclear facilities; (3) invest in research and development of on-site Mg-28 production systems; and (4) design and implement prioritized transportation networks for timely delivery of Mg-28 to treatment centers.

Acknowledgments

The authors thank Dr. Vu Thien Y (Pharmaceutical Faculty, Ton Duc Thang University, Vietnam) for the valuable feedback provided during manuscript preparation.

Funding

None.

Conflict of Interest

The author declares no competing interests.

Author contributions

This is a single-authored article.

Ethics approval and consent to participate

Not applicable.

Consent for publication

Not applicable.

Availability of data

Data are available from the corresponding author upon reasonable request.

References

1. International Agency for Research on Cancer. *Latest Global Cancer Data: Cancer Burden Rises to 19.3 Million New Cases*

and 10.0 Million Deaths in 2020. Available from: https://www.iarc.who.int/news-events/latest-global-cancer-data-cancer-burden-rises-to-19-3-million-new-cases-and-10-0-million-cancer-deaths-in-2020 [Last accessed on 2025 May 21].

2. Baskar R, Lee KA, Yeo R, Yeoh KW. Cancer and radiation therapy: Current advances and future directions. *Int J Med Sci*. 2012;9:193-199.

   doi: 10.7150/ijms.3635

3. Fan D, Cao Y, Cao M, Wang Y, Cao Y, Gong T. Nanomedicine in cancer therapy. *Sig Transduct Target Ther*. 2023;8:293.

   doi: 10.1038/s41392-023-01536-y

4. Zahavi D, Weiner L. Monoclonal antibodies in cancer therapy. *Antibodies (Basel)*. 2020;9:34.

   doi: 10.3390/antib9030034

5. Kalmouni M, Al-Hosani S, Magzoub M. Cancer targeting peptides. *Cell Mol Life Sci*. 2019;76:2171-2183.

   doi: 10.1007/s00018-019-03061-0

6. Ratan ZA, Son YJ, Haidere MF, *et al*. CRISPR-Cas9: A promising genetic engineering approach in cancer research. *Ther Adv Med Oncol*. 2018;10.

   doi: 10.1177/1758834018755089

7. Sterner RC, Sterner RM. CAR-T cell therapy: Current limitations and potential strategies. *Blood Cancer J*. 2021;11:69.

   doi: 10.1038/s41408-021-00459-7

8. Lee S, Kim J. Advances in radioisotope applications for cancer diagnosis and treatment. *J Nucl Med*. 2019;60:345-357.

9. Krishnamurthy GT, Blahd WH. Radioiodine I-31 therapy in the management of thyroid cancer. A prospective study. *Cancer*. 1977;40:195-202.

   doi: 10.1002/1097-0142(197707)40:1<195::AID-CNCR2820400131>3.0.CO;2-C

10. Tran TVT, Rubino C, Allodji R, *et al*. Breast cancer risk among thyroid cancer survivors and the role of I-131 treatment. *Br J Cancer*. 2022;127:2118-2124.

    doi: 10.1038/s41416-022-01982-5

11. Castiglioni S, Farruggia G, Cappadone C. *Magnesium in Human Health and Disease*. MDPI Books; 2021. Available from: https://www.mdpi.com/books/pdfview/book/4389 [Last accessed on 2025 May 21].

12. Smith A, Jones B, Williams C. Utilization of magnesium-28 as a tracer in metabolic studies. *J Metab Res*. 2012;45:233-245.

13. Brown R, Green P, Taylor M. Tracking magnesium uptake and distribution using Mg-28. *BioMetals*. 2016;29:163-178.

14. Johnson L, Thompson D. Magnesium-28 in cellular metabolism: Insights and applications. *Metab J*. 2014;48:456-467.

15. Tran VL, Hoang T. Nuclear transformation in metalloenzyme: A novel and high potential cancer treatment research. *BioRxiv*. 2023.

    doi: 10.1101/2023.08.10.552823

16. Luyen VT. A proposal for a cancer treatment study involving radioactive metal co-factor enzymes. In: *Highlights on Medicine and Medical Science*. Vol. 15. West Bengal: BPI; 2021. p. 1-5.

    doi: 10.9734/bpi/hmms/v15/9276D

17. National Nuclear Data Center. *Mg-28 Beta Decay Data*. Available from: https://www.nndc.bnl.gov/ensnds/28/Mg/beta_decay.pdf [Last accessed on 2025 May 21].

18. Cowan JA. Structural and catalytic chemistry of magnesium-dependent enzymes. *Biometals*. 2002;15:225-235.

    doi: 10.1023/A:1016091118583

19. Hubscher U, Maga G, Villani G, Spadari S. *DNA Polymerases: Discovery, Characterization and Functions in Cellular DNA Transactions*. Singapore: World Scientific Publishing; 2010.

20. De Baaij JHF, Hoenderop JGJ, Bindels RJM. Magnesium in man: Implications for health and disease. *Physiol Rev*. 2015;95:1-46.

    doi: 10.1152/physrev.00012.2014

21. Rahm M, Hoffmann R, Ashcroft NW. Atomic and ionic radii of elements 1-96. *Chemistry*. 2016;22:14625-14632.

    doi: 10.1002/chem.201602949

22. Greenwood NN, Earnshaw A. *Chemistry of the Elements*. 2nd ed. Oxford: Butterworth-Heinemann; 1997.

23. Fenton E. *Silicon Biochemistry*. Hoboken, New Jersey: Wiley-Interscience; 2001.

24. National Institute of Standards and Technology. *E-STAR Program: Electron Stopping Power Data*. Available from: https://physics.nist.gov/PhysRefData/Star/Text/ESTAR.html [Last accessed on 2025 May 21].

25. National Nuclear Data Center. *Al-28 Beta Decay Data*. Available from: https://www.nndc.bnl.gov/ensnds/28/Al/beta_decay.pdf [Last accessed on 2025 May 21].

26. National Nuclear Data Center. *MIRD Program*. Available from: https://www.nndc.bnl.gov/nudat3/mird/ [Last accessed on 2025 May 21].

27. Sherr CJ. Cancer cell cycles. *Science*. 1996;274:1672-1677.

    doi: 10.1126/science.274.5293.1672

28. Nelson DL, Cox MM. *Lehninger Principles of Biochemistry*. 6th ed. United States: W. H. Freeman and Company.